Energy & Environmental Science

COMMUNICATION

View Article Online
View Journal | View Issue

Cite this: *Energy Environ. Sci.*, 2017, **10**, 516

Received 8th October 2016,
Accepted 16th December 2016

DOI: 10.1039/c6ee02941h

www.rsc.org/ees

Scaling behavior of moisture-induced grain degradation in polycrystalline hybrid perovskite thin films†

Qi Wang,‡ Bo Chen,‡ Ye Liu, Yehao Deng, Yang Bai, Qingfeng Dong and Jinsong Huang*

The stability of perovskite solar cells has shown a huge variation with respect to the film process and film morphology, while the underlining mechanism for the morphology-dependent degradation of the perovskite film has remained elusive. Herein, we report a scaling behavior of moisture-induced grain degradation in polycrystalline $CH_3NH_3PbI_3$ films. The degradation rates of $CH_3NH_3PbI_3$ films in moisture were shown to be sensitive to the grain sizes. The duration that was needed for different films to degrade by the same percent showed a linear relationship with the grain size, despite the fact that the films were formed by five different deposition methods. This scaling behavior can be explained by the degradation along the in-plane direction, which is initiated at the grain boundary (GB). The GBs of $CH_3NH_3PbI_3$ films consist of an amorphous intergranular layer, which allows quick diffusion of moisture into the perovskite films. It was found that thermal annealing induced surface self-passivation plays a critical role in stabilizing the surfaces of thin films and single crystals by reducing the moisture-sensitive methylammonium ions at the surface. The determination of the scaling behavior of grain degradation highlights the importance of stabilizing the GBs to improve the stability of perovskite solar cells.

Broader context

Harnessing solar energy to solve the world energy crisis has been persistently pursued in the past several decades. In the past, organic–inorganic halide perovskite (OIHP) solar cells have been revolutionizing the photovoltaic field due to their rapid increase in efficiency to over 22%, low material and fabrication costs, and scalable manufacturing capability. However, the instability of OIHP materials, particularly their poor moisture stability due to their phenomenal hydroscopic nature, remains a huge obstacle for the commercialization of this technology. Thus far, most previous studies have reported the increased moisture stability of perovskite solar cells by depositing moisture-blocking layers on perovskites. However, the intrinsic moisture stability of OIHP materials has not been studied in detail particularly with respect to the grain morphology. In this study, we revealed the critical role of grain boundary defects in accelerating the moisture-induced degradation of OIHP polycrystalline films. Significantly increased moisture stability was observed in OIHP films with a larger grain size, which demonstrated a way of increasing the intrinsic stability of OIHP materials. Increasing the grain size is also needed for increasing the efficiency of OIHP solar cells because large grains and grain boundary passivation are also needed to suppress the charge recombination at grain boundaries.

Introduction

Organic–inorganic halide perovskite (OIHP) materials have drawn tremendous attention since the power conversion efficiency (PCE) of OIHP solar cells skyrocketed from 3.8% to a certified 22.1% in the past few years, which is already at par with other commercialized thin film photovoltaic technologies.[1–10] These materials have excellent properties of defect tolerance,[11] strong optical absorption,[12] low trap density,[8] and a long carrier diffusion length, which is much longer than the optical absorption length.[13,14] Their prospects for the next generation of low-cost photovoltaics are enabled by their natural abundance, low-cost raw materials, and low-energy solution process. Nevertheless, concerns about the poor stability of OIHP materials, particularly their poor moisture stability due to their phenomenal hydroscopic nature, are hindering the commercialization of these materials.[15–18] In contrast to the enhancement of the PCE, understanding the intrinsic stability of OIHP lags far behind.

The degradation observed in OIHP solar cells was frequently attributed to the intrinsic low stability of OIHP materials, which is caused by their low formation energy and hydroscopic nature, and thus good device encapsulation is necessary for long-term device operation. On the other hand, the reported stability of perovskite solar cells from different groups has demonstrated a large variation over a period of hours to months even for encapsulated devices and films,[6,16,19,20] which implies that OIHP materials might not be that intrinsically unstable. One very encouraging observation by us was that

Department of Mechanical and Materials Engineering, University of Nebraska-Lincoln, Lincoln, Nebraska 68588, USA. E-mail: jhuang2@unl.edu

† Electronic supplementary information (ESI) available. See DOI: 10.1039/c6ee02941h

‡ Q. W. and B. C. contributed equally to this work.

some perovskite single crystals were very stable in air. The $CH_3NH_3PbI_3$ ($MAPbI_3$) single crystals synthesized 2–3 years ago for a study of the carrier intrinsic diffusion length still have a black color and shiny crystal facets without notable degradation (ESI,† Fig. S1) despite being stored in ambient atmosphere without any encapsulation. This better stability of the single crystals also implies that the faster device degradation observed in polycrystalline perovskite solar cells might be directly related to the perovskite grain size or grain boundaries (GBs). Understanding the correlation of the grain size or GB with the perovskite stability is important in order to enhance the stability of future perovskite solar cells because the grain size can be significantly tuned by advanced film fabrication processes.[21–23]

In this study, we discovered that the moisture stability of $MAPbI_3$ polycrystalline films follows a scaling behavior with grain sizes, with significantly increased stability observed in films with larger grains. The GBs in $MAPbI_3$ thin films play a critical role in initiating film degradation in a moist environment, where the moisture permeates or reacts with the GBs quicker than with the top surface of the grains. The fast infiltration of moisture was related to the structure of the GBs, which consists of an amorphous intergranular film (IGF) with a thickness around 5 nm.

Results and discussion

To reveal the relation between perovskite grain size and film moisture stability, $MAPbI_3$ films with different grain sizes were formed by controlling the thermal annealing time, and the degradation process of these films was studied in a controlled humid environment. The $MAPbI_3$ films were formed by the two-step inter-diffusion method on poly(triaryl amine) (PTAA) covered ITO substrates.[24] The film thickness was fixed at ~500 nm. Grain coarsening by thermal annealing is a general method to tune the grain size of thin films, and was demonstrated to be effective for perovskite thin films as well.[21,25] As shown in the ESI,† Fig. S2 and S3, the average grain sizes of $MAPbI_3$ films annealed for 15 min, 30 min, 60 min, 90 min and 120 min were 297 nm, 450 nm, 522 nm, 613 nm, 678 nm, respectively. Then, $MAPbI_3$ samples with different grain sizes were stored in a set-up shown in ESI,† Fig. S4, and the humidity was controlled to be 85% ± 5% by adjusting the N_2 gas flow rate, which could also exclude the influence of oxygen. Photographic images in Fig. 1a recorded the degradation process of these $MAPbI_3$ films in moisture. The degradation process of $MAPbI_3$ films was well observed with the color change of the films from black to colorless, which was characterized by the formation of

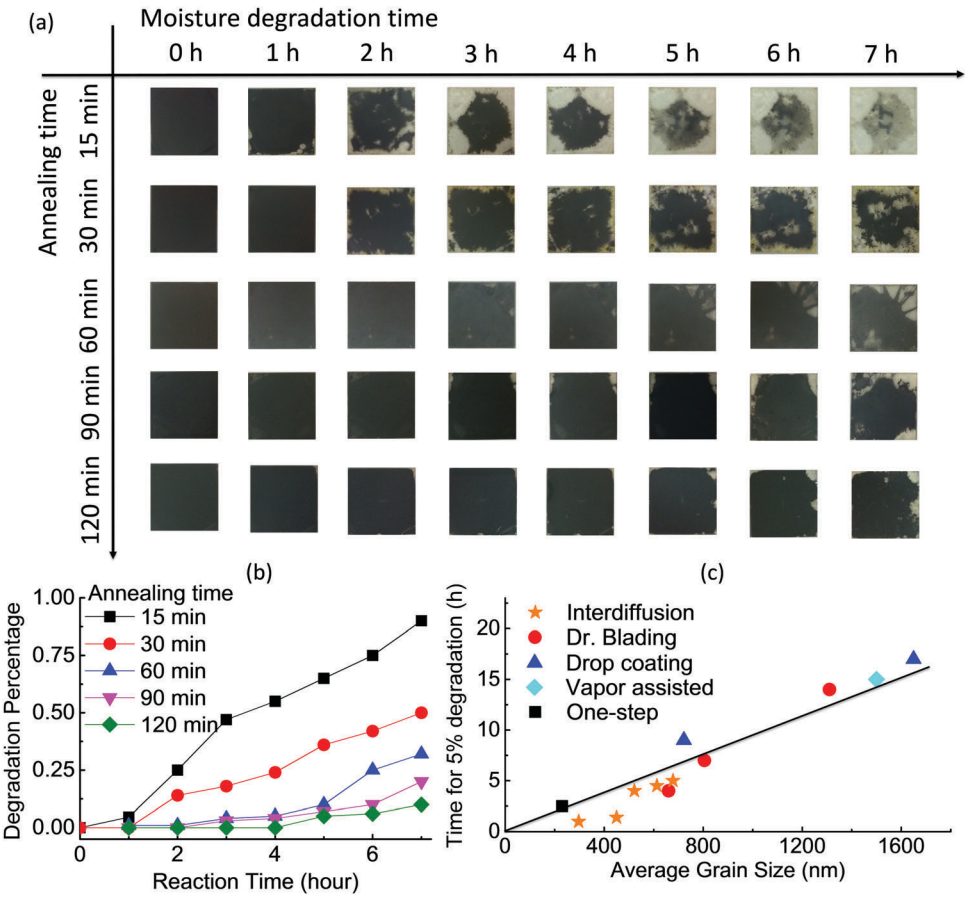

Fig. 1 Scaling behavior of the $MAPbI_3$ films degradation. (a) Photographs of the perovskite films stored in 85% humidity for different times. The films were formed by a two-step inter-diffusion method while undergoing different annealing times; (b) degradation percentage of the perovskite films with different thermal annealing times. (c) Time needed for degradation of the perovskite films by 5%, which were fabricated by different methods.

hydrated perovskite phases.[26–28] This decoloring process was assigned to the initial stage of moisture-induced degradation of perovskite into monohydrate $CH_3NH_3PbI_3{\cdot}H_2O$, and further conversion to dihydrate $(CH_3NH_3)_4PbI_6{\cdot}2H_2O$ with additional moisture and time, which further degraded to PbI_2 and MAI upon enough moisture exposure time.[29] $CH_3NH_3PbI_3{\cdot}H_2O$ was reported to be able to convert back to black $CH_3NH_3PbI_3$ upon drying; however the process was not fully reversible after it was converted to dihydrate.[28] Our study also confirmed that the decoloring process was reversible at the initial stage of degradation when the degraded area was 5–10%, whereas it became irreversible when the degraded area exceeded 30% of the total area after long exposure to moisture (ESI,† Fig. S5). Herein, we only consider the worst case of moisture-induced perovskite degradation (*i.e.*, under continuous exposure to moisture) because there was no protocol to follow for the testing of the recovery of a solar panel with periodic drying and moisture soaking. The degradation behavior of these $MAPbI_3$ films can be summarized as follows: first, the films annealed for longer time with larger grain sizes had better resistance to moisture and degraded slower; second, the degradation process was initiated at certain spots on the films and subsequently expanded to their surrounding area along the in-plane direction. By measuring the ratio of the decolored area to the entire film area, we derived the degradation percentages of the perovskite films at different moisture exposure times. Details about the method for degradation area measurements and the degradation percentage calculation can be found in ESI,† Fig. S6. Fig. 1b clearly shows that the perovskite samples with smaller grain sizes degraded quicker. The film prepared by the shortest annealing time of 15 min with an average grain size of 297 nm degraded faster than other films with ~85% of its total area degraded after exposure to a moist environment for 7 hours. The perovskite film with an average grain size of 678 nm only degraded ~10% after being stored at the same humidity for 7 hours. The strong correlation between grain size and moisture stability is clearly shown in Fig. 1c, which summarizes the time needed for the samples to degrade 5% ($t_{0.05}$) of their areas when exposed to ~85% moisture. It is clear that samples with large grains take a longer time to degrade than the samples with smaller grains. More interestingly, $t_{0.05}$ of different films almost followed a linear relationship with the grain sizes, which is defined as a scaling behavior of perovskite grain degradation.

To verify the scaling behavior of $MAPbI_3$ grain degradation, we studied the grain degradation in moisture for the perovskite films fabricated *via* four other reported methods, including one-step spin-coating,[30,31] doctor-blading,[23] vapor-assisted solution process (VASP)[32] and drop-coating.[33] Details about the film fabrication *via* the four methods can be found in the ESI.† The scanning electron microscopy (SEM) images and grain size distributions of the films fabricated *via* each method are shown in ESI,† Fig. S7 and S8. The average grain sizes of different films ranged from ~200 nm to ~1600 nm. Degradation curves and photographs of each film during ~85% moisture treatment are shown in ESI,† Fig. S9 and S10, respectively. The time needed for 5% degradation of their total area is summarized in Fig. 1c. It was found that all of the data was astonishingly and approximately located on a straight line which was fit with a linear regression with an *R*-squared value of 0.96, confirming the universal scaling behavior of the moisture induced grain degradation. The universal scaling behavior could be further confirmed by examining $t_{0.1}$, $t_{0.15}$, and $t_{0.2}$, which are shown in ESI,† Fig. S11. All the points in the figures were located around a straight line and were fit with a linear regression with *R*-squared values close to or above 0.9.

The scaling behavior of moisture-induced degradation in $MAPbI_3$ films can be modeled with assumptions that the grain degradation initiates at the GBs and the grains degrade along the in-plane direction rather than the out-of-plane direction, which is illustrated in Fig. 2a. From the top-view of a film (ESI,† Fig. S12), the grain size of the film has an inverse relationship with the total length of the grain boundary. Since the moisture-induced degradation starts from the perovskite GBs, the degradation rate was derived to be proportional to the grain size. Details about this model and the derived equation are given in the ESI.† The time needed for degradation of 5% of the total film area (S) was calculated as follows:

$$t_{0.05} = \frac{a}{4v} \times \frac{\Delta S}{S} = \frac{a}{80v} \quad (1)$$

where ΔS is the degraded area, a is the average grain size, and v is the grain degradation rate. This equation shows that the degradation rate of perovskite films is proportional to the grain size, and provides the theory for the observed scaling behavior of grain degradation. Based on this equation, we can also derive an average grain degradation rate of ~0.8 nm h^{-1} for $MAPbI_3$ films at the initial stage under a humidity of 85% ± 5% from Fig. 1c.

The faster in-plane degradation of $MAPbI_3$ grains in moisture seems counter-intuitive, because both grain top surface and GBs are exposed to moisture. Nevertheless, it was supported by other independent studies, such as the degradation rate independent of the film's thickness. In this study, we fabricated several perovskite films with different thicknesses ranging from 450 nm to 1000 nm *via* the same inter-diffusion method. The SEM images of these films are shown in ESI,† Fig. S13, where the average grain sizes range from 660 nm to 840 nm. These films showed similar degradation rates in moisture, as shown in the Fig. 2b and ESI,† Fig. S14. If the degradation of films was along the out-of-plane direction, the 450 nm-thick film would have degraded two times faster than the 1000 nm-thick film. The degradation of the grains along the in-plane direction could be explained by the continuous permeation of moisture into the interface perovskite/hydrated perovskite, which is irregular and defective. In this sense, the surface of the perovskite films must be free of moisture-sensitive defects. A theoretical study has predicted that the PbI_2-terminated perovskite surface is more resistant to degradation caused by moisture due to the stronger Pb–I bond[34] and much lower solubility of PbI_2 in water than that of methylammonium (MA) ions. This caused us to speculate that the slowly – degradation of the perovskite film surface could be terminated with more Pb–I bonds, which is more resistant to moisture. This is reasonable because thermal annealing, which is a process that is needed for almost every film formation,

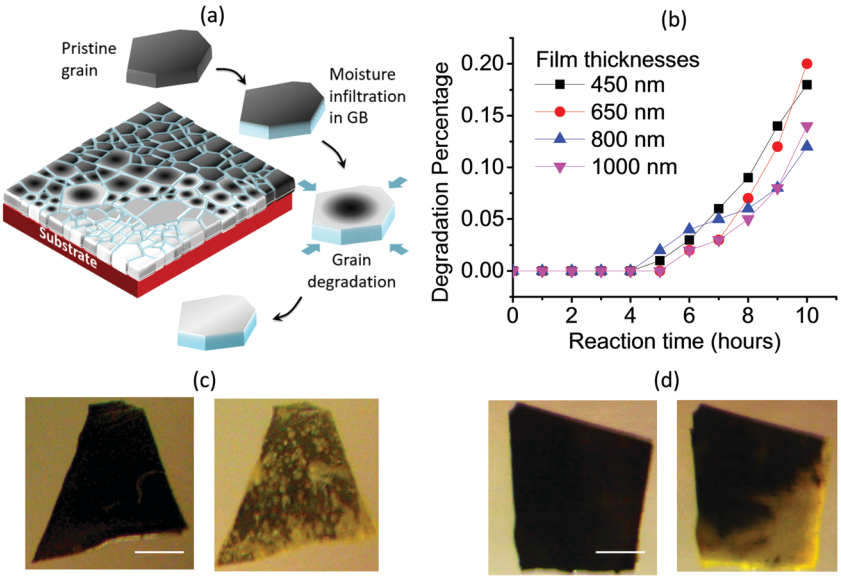

Fig. 2 Degradation of $MAPbI_3$ films in moisture along the in-plane direction. (a) Schematic diagram showing the degradation of the perovskite film in moisture. The grain degradation is initiated at certain grain boundaries of the films and followed by the further expansion of those spots to the surrounding area of the films along the in-plane direction. (b) Degradation percentage of the $MAPbI_3$ films with different thickness. The films were formed by a two-step inter-diffusion method. (c and d) Photographs of the thin single crystals without (c) and with (d) thermal annealing before testing. The scale bar in the image (c) and (d) is 1 mm.

should drive the leaving of MA ions or MAI from the surface due to weak bonding between MA^+ with other ions. To verify this, we compared the degradation behavior of two thin single crystals, while one of them was annealed at 100 °C for 2 hours. We recently developed a new solution method to grow $MAPbI_3$ thin single crystals with a 1–2 mm lateral size and ~20 μm thickness, which provided a good platform to study the degradation process of perovskite grain. The method of growing high-aspect-ratio single crystals will be published elsewhere. For a fair comparison, one single crystal was cut into two halves and one of them was annealed under the typical annealing condition in the polycrystalline film fabrication. After that, the annealed sample was further cut along the edge to expose the fresh $MAPbI_3$ on the edge. The degradation process of the two pieces of single crystals was recorded (Fig. 2c and d). It was found that the degradation of the annealed crystal started from the edge of the sample, followed by the in-plane expansion of the degraded area from one side to the other. In contrast, the sample without post-annealing degraded more uniformly, verifying that the annealing of perovskite films or single crystals did suppress the degradation of the surface.

The scaling behavior for the degradation of $MAPbI_3$ polycrystalline films and the excellent stability of single crystals implies that the GBs in perovskite materials should play a critical role in initiating the moisture-induced degradation process. We examined the structure of $MAPbI_3$ GBs with high resolution transmission electron microscopy (HRTEM) and scanning transmission electron microscopy (STEM). The sample was prepared *via* a focused ion beam (FIB). It was critical to use a small ion beam current and a small acceleration voltage of 5 kV in the milling process to minimize the thermal damage induced by a focused ion beam.[35] Fig. 3a shows a schematic of the perovskite grain and GBs. Fig. 3b shows the STEM cross-section image of one typical sample, where the GB could be clearly identified. The HRTEM image in Fig. 3c shows that the two grains have different orientations. The zone axes (ZA) of the two grains are indexed to be [010] and [110], respectively, based on the fast Fourier transformation (FFT) of lattices and simulated diffraction patterns shown in ESI,† Fig. S15. Interestingly, an amorphous region with a thickness of ~5 nm was found between the two neighboring grains. To the best of our knowledge, this is the first time the detailed structure of $MAPbI_3$ GBs has been revealed, which showed clear evidence for the presence of an amorphous region in the GBs of $MAPbI_3$ films. On the other hand, a similar amorphous structure at GBs, often called an intergranular film, has been frequently observed in other polycrystalline ceramics, metals and oxides.[36–38] A previous study reported that impurity segregation in GBs is accompanied with the formation of IGF in doped ceramics.[37] The formation of IGF in solution-processed $MAPbI_3$ films may be related to its non-stoichiometric composition and the segregation of the non-stoichiometric excess residuals into the GBs. Recently, Park *et al.* reported that adding excess MAI in the perovskite precursor yielded the formation of a MAI layer at the GBs, which was explained by the extraction of a non-stoichiometric excess of MAI into GBs during grain coarsening.[39] Therefore, the perovskite films with a non-stoichiometric composition should have a thicker IGF and may degrade faster than films with a stoichiometric composition. This speculation could be justified by our frequent observation that inter-diffusion films degrade slightly faster than what is predicted from the fitted line (Fig. 1c and ESI,† Fig. S11). The unique fabrication process of the inter-diffusion method, where the MAI solution was

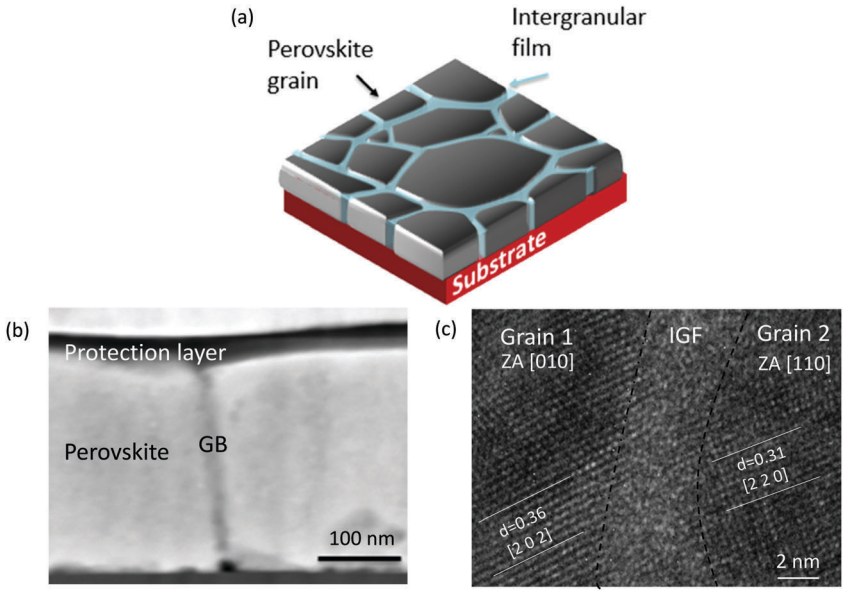

Fig. 3 Amorphous intergranular films at the grain boundary of $MAPbI_3$. (a) Schematic showing the intergranular film in grain boundaries. (b) A STEM cross-section image of the perovskite sample. (c) A HRTEM cross-section image revealing the presence of an intergranular film between two neighboring grains. The lattice fringes and zone axis of each grain were indexed according to the simulated results of diffraction patterns shown in the ESI.†

dropped on PbI_2 films, could cause excess MAI to be left in the perovskite films because there was more than enough MAI in the solution to react with PbI_2 films. The non-stoichiometric excess of MAI in inter-diffusion films may cause the IGF to be much thicker than that of the films made by other methods, where equal molar ratios of MAI and PbI_2 were premixed in the precursor solution. In this context, it is speculated that the perovskite films with a stoichiometric composition should have the thinnest IGF, which may be a new strategy to suppress the influence of IGF on the stability of perovskite films.

We hypothesized that the amorphous and defective region at GBs facilitates the quick permeation of moisture along the GBs due to the relative more open structure than the crystalline region (Fig. 4a). To verify this, STEM based energy dispersive X-ray spectroscopy (STEM/EDS) was conducted to trace the permeation of moisture by mapping the oxygen distribution after a polycrystalline $MAPbI_3$ film with an average grain size of 300 nm was exposed in moisture for 0.5 h. Molecular oxygen from air can be excluded because the moisture was introduced by N_2 as the carrying gas. Details about the STEM/EDS sample fabrication are found in the ESI.† Fig. S16 (ESI†) shows the oxygen distribution of the $MAPbI_3$ film before the moisture exposure. The EDS signal intensity of the pristine sample was uniformly distributed. By contrast, Fig. 4b and c show the high angle annular dark field (HAADF) STEM image of a $MAPbI_3$ film after moisture exposure and the corresponding EDS mapping of elemental oxygen at the same location. It was found that GBs had a higher content of water compared with the grain interior. The fast permeation of water at GBs is clearer in Fig. 4d, which is the oxygen distribution image overlaid with the morphology STEM image. This conclusively confirmed that the moisture permeates into perovskite films through amorphous GBs and initiates the degradation.

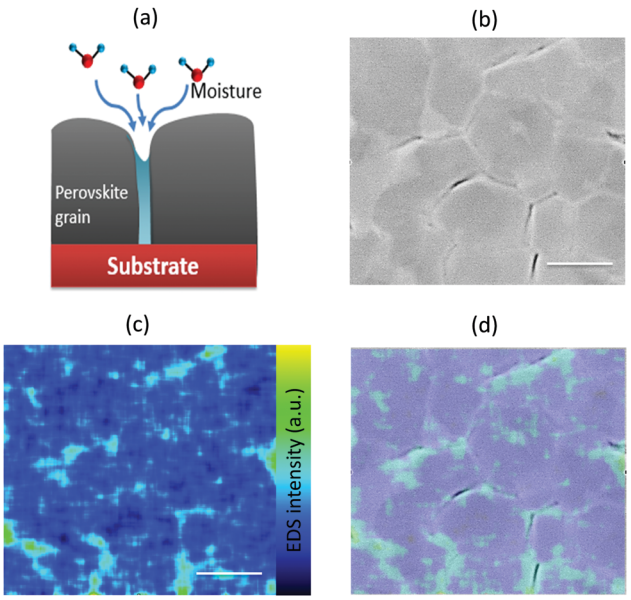

Fig. 4 STEM/EDS studies of fast infiltration/reaction of moisture with perovskite grain boundaries. (a) Schematic showing the interaction of moisture with a bare perovskite film. An STEM image of perovskite film (b) and an EDS oxygen element mapping image (c) showing the distributions of elemental oxygen in the film. The scale bar in image (b) and (c) is 500 nm. (d) Overlap of EDS mapping image with STEM image.

Other possibilities that may also change the moisture stability of the perovskite films were also considered to find out whether the scaling behavior could be explained by these factors, such as surface roughness, grain orientation and crystallinity. The role of surface roughness on moisture stability could be observed by comparing the moisture stability of doctor blading films and spin coating films. It has been well established by us that films made

by the doctor blading method are rougher than spun films because of the formation of large domains and a concentric ring structure.[23,40] However, as shown in Fig. 1c, when the films made by these two methods have comparable grain sizes, they show similar moisture stability, indicating that film roughness does not cause the scaling behavior. Grain orientation was another factor that may change the perovskite film stability. Certain grains in the films may degrade faster than others because different grain facets were predicted to have different degradation rates. Our previous X-ray diffraction (XRD) studies showed that the spun perovskite films made *via* the inter-diffusion method had a random grain orientation,[24] while the doctor blading films had the preferred (2 2 0) orientation.[23] Nevertheless the doctor blading films showed a similar degradation rate (Fig. 1c) with the inter-diffusion films when they had a comparable grain size, which indicates that the grain orientation cannot explain the difference in moisture stability. It is noted that the difference in the thermal annealing time in sample preparation may also cause the change of crystallinity of the perovskite grains. However point defects inside the grains should not impact moisture stability because moisture needs to permeate into the grain from the surface or GBs.

Conclusion

We reported the scaling behavior of the moisture-induced grain degradation in polycrystalline perovskite thin films. It was found that the grain boundary in $MAPbI_3$ consisted of an amorphous film, which absorbs/reacts with water molecules much faster than the grain surface. The moisture stability of perovskite materials has become one of the biggest hindrances for the commercialization of perovskite solar cells. Our study not only sheds light on the perovskite degradation mechanism by revealing the critical role of defects in accelerating the degradation of perovskite, but also suggests a method to further increase the moisture stability by increasing the grain size of perovskite films and improving the quality of the GBs by remedying the amorphous region to prevent moisture infiltration. This is consistent with the route to make high efficiency solar cells because the large grains and grain boundary passivation are also needed to suppress the charge recombination at GBs. In addition, reducing the IGF thickness during the film formation process could also enhance the stability of perovskite films. Tuning the composition of the perovskite films (not the composition of the perovskite precursors) to be stoichiometric may significantly reduce the IGF thickness or even totally eliminate IGF in the perovskite films. Using a high purity precursor may be another effective approach, if the formation of the amorphous region is demonstrated to be related to the impurities in the precursor. Finally, we think that grain boundary healing can also be an effective way to enhance not only the stability but also the efficiency of perovskite solar cells, while understanding that the nature of grain boundary defects will be crucial before an effective method is proposed.

Acknowledgements

This study was supported by the National Science Foundation (DMR-1505535), Department of Energy (DE-EE0006709), and Office of Naval Research (N00014-15-1-2713).

References

1 M. A. Green, A. Ho-Baillie and H. J. Snaith, *Nat. Photonics*, 2014, **8**, 506–514.
2 M. D. McGehee, *Nat. Mater.*, 2014, **13**, 845–846.
3 W. S. Yang, J. H. Noh, N. J. Jeon, Y. C. Kim, S. Ryu, J. Seo and S. I. Seok, *Science*, 2015, **348**, 1234–1237.
4 W. Chen, Y. Wu, Y. Yue, J. Liu, W. Zhang, X. Yang, H. Chen, E. Bi, I. Ashraful and M. Grätzel, *Science*, 2015, **350**, 944–948.
5 H. Zhou, Q. Chen, G. Li, S. Luo, T.-b. Song, H.-S. Duan, Z. Hong, J. You, Y. Liu and Y. Yang, *Science*, 2014, **345**, 542–546.
6 J. Burschka, N. Pellet, S.-J. Moon, R. Humphry-Baker, P. Gao, M. K. Nazeeruddin and M. Grätzel, *Nature*, 2013, **499**, 316–319.
7 M. Liu, M. B. Johnston and H. J. Snaith, *Nature*, 2013, **501**, 395–398.
8 T. M. Brenner, D. A. Egger, L. Kronik, G. Hodes and D. Cahen, *Nat. Rev. Mater.*, 2016, **1**, 15007.
9 NERL, http://www.nrel.gov/ncpv/images/efficiency_chart.jpg.
10 H.-S. Kim, C.-R. Lee, J.-H. Im, K.-B. Lee, T. Moehl, A. Marchioro, S.-J. Moon, R. Humphry-Baker, J.-H. Yum and J. E. Moser, *Sci. Rep.*, 2012, **2**, 591.
11 W.-J. Yin, T. Shi and Y. Yan, *Appl. Phys. Lett.*, 2014, **104**, 063903.
12 Z. Xiao, Y. Yuan, Q. Wang, Y. Shao, Y. Bai, Y. Deng, Q. Dong, M. Hu, C. Bi and J. Huang, *Mater. Sci. Eng., R*, 2016, **101**, 1–38.
13 S. D. Stranks, G. E. Eperon, G. Grancini, C. Menelaou, M. J. Alcocer, T. Leijtens, L. M. Herz, A. Petrozza and H. J. Snaith, *Science*, 2013, **342**, 341–344.
14 C. Wehrenfennig, G. E. Eperon, M. B. Johnston, H. J. Snaith and L. M. Herz, *Adv. Mater.*, 2014, **26**, 1584–1589.
15 X. Li, M. I. Dar, C. Yi, J. Luo, M. Tschumi, S. M. Zakeeruddin, M. K. Nazeeruddin, H. Han and M. Grätzel, *Nat. Chem.*, 2015, **7**, 703–711.
16 T. A. Berhe, W.-N. Su, C.-H. Chen, C.-J. Pan, J.-H. Cheng, H.-M. Chen, M.-C. Tsai, L.-Y. Chen, A. A. Dubale and B.-J. Hwang, *Energy Environ. Sci.*, 2016, **9**, 323–356.
17 G. Niu, X. Guo and L. Wang, *J. Mater. Chem. A*, 2015, **3**, 8970–8980.
18 S. Yang, Y. Wang, P. Liu, Y.-B. Cheng, H. J. Zhao and H. G. Yang, *Nat. Energy*, 2016, **1**, 15016.
19 Y. Han, S. Meyer, Y. Dkhissi, K. Weber, J. M. Pringle, U. Bach, L. Spiccia and Y.-B. Cheng, *J. Mater. Chem. A*, 2015, **3**, 8139–8147.
20 D. Bi, P. Gao, R. Scopelliti, E. Oveisi, J. Luo, M. Grätzel, A. Hagfeldt and M. K. Nazeeruddin, *Adv. Mater.*, 2016, **28**, 2910–2915.
21 C. Bi, Y. Shao, Y. Yuan, Z. Xiao, C. Wang, Y. Gao and J. Huang, *J. Mater. Chem. A*, 2014, **2**, 18508–18514.

22 C. Bi, Q. Wang, Y. Shao, Y. Yuan, Z. Xiao and J. Huang, *Nat. Commun.*, 2015, **6**, 7747.
23 Y. Deng, E. Peng, Y. Shao, Z. Xiao, Q. Dong and J. Huang, *Energy Environ. Sci.*, 2015, **8**, 1544–1550.
24 Z. Xiao, C. Bi, Y. Shao, Q. Dong, Q. Wang, Y. Yuan, C. Wang, Y. Gao and J. Huang, *Energy Environ. Sci.*, 2014, **7**, 2619–2623.
25 M. Saliba, K. W. Tan, H. Sai, D. T. Moore, T. Scott, W. Zhang, L. A. Estroff, U. Wiesner and H. J. Snaith, *J. Phys. Chem. C*, 2014, **118**, 17171–17177.
26 Z. Zhu, V. G. Hadjiev, Y. Rong, R. Guo, B. Cao, Z. Tang, F. Qin, Y. Li, Y. Wang and F. Hao, *Chem. Mater.*, 2016, **28**, 7385–7393.
27 J. A. Christians, P. A. Miranda Herrera and P. V. Kamat, *J. Am. Chem. Soc.*, 2015, **137**, 1530–1538.
28 J. Yang, B. D. Siempelkamp, D. Liu and T. L. Kelly, *ACS Nano*, 2015, **9**, 1955–1963.
29 A. l. M. Leguy, Y. Hu, M. Campoy-Quiles, M. I. Alonso, O. J. Weber, P. Azarhoosh, M. Van Schilfgaarde, M. T. Weller, T. Bein and J. Nelson, *Chem. Mater.*, 2015, **27**, 3397–3407.
30 M. Xiao, F. Huang, W. Huang, Y. Dkhissi, Y. Zhu, J. Etheridge, A. Gray-Weale, U. Bach, Y. B. Cheng and L. Spiccia, *Angew. Chem.*, 2014, **126**, 10056–10061.
31 B. Chen, Y. Bai, Z. Yu, T. Li, X. Zheng, Q. Dong, L. Shen, M. Boccard, A. Gruverman and Z. Holman, *Adv. Energy Mater.*, 2016, **6**, 1601128.
32 Q. Chen, H. Zhou, Z. Hong, S. Luo, H.-S. Duan, H.-H. Wang, Y. Liu, G. Li and Y. Yang, *J. Am. Chem. Soc.*, 2013, **136**, 622–625.
33 A. Mei, X. Li, L. Liu, Z. Ku, T. Liu, Y. Rong, M. Xu, M. Hu, J. Chen and Y. Yang, *Science*, 2014, **345**, 295–298.
34 E. Mosconi, J. M. Azpiroz and F. De Angelis, *Chem. Mater.*, 2015, **27**, 4885–4892.
35 N. I. Kato, *J. Electron Microsc.*, 2004, **53**, 451–458.
36 A. Subramaniam, C. T. Koch, R. M. Cannon and M. Rühle, *Mater. Sci. Eng., A*, 2006, **422**, 3–18.
37 V. K. Gupta, D.-H. Yoon, H. M. Meyer and J. Luo, *Acta Mater.*, 2007, **55**, 3131–3142.
38 R. Brydson, S. C. Chen, F. L. Riley, S. J. Milne, X. Pan and M. Rühle, *J. Am. Ceram. Soc.*, 1998, **81**, 369–379.
39 D.-Y. Son, J.-W. Lee, Y. J. Choi, I.-H. Jang, S. Lee, P. J. Yoo, H. Shin, N. Ahn, M. Choi and D. Kim, *Nat. Energy*, 2016, **1**, 16081.
40 Y. Deng, Q. Wang, Y. Yuan and J. Huang, *Mater. Horiz.*, 2015, **2**, 578–583.

